Eur. Phys. J. D **17**, 337–344 (2001)

THE EUROPEAN PHYSICAL JOURNAL D

EDP Sciences

Tomographic determination of plasma velocity with the use of ion Doppler spectroscopy

A.L. Balandin[a] and Y. Ono[b]

High Temperature Plasma Center, University of Tokyo, 2–11–16 Yayoi, Bunkyo–ku, Tokyo 113–8656, Japan

Received 10 March 2001 and Received in final form 25 July 2001

Abstract. An inversion method for ion Doppler shift of spectrum lines was developed for plasma velocity measurements. By reducing the problem to the vectorial Radon transform, the characteristics of plasma ion velocity distribution such as vector potential/vorticity and velocity components were computed in two-dimensional space. Computer simulation of the reconstruction of different vector potential (vector field) models gives evidence that the reconstruction errors are acceptable, and the method can surely be used for real experimental data.

PACS. 07.05.Tp Computer modeling and simulation – 02.60.Cb Numerical simulation; solution of equations – 52.70.Kz Optical (ultraviolet, visible, infrared) measurements

1 Introduction

The Doppler shift and broadening effects are often used as spectroscopic measurement techniques of important plasma parameters. Spectral line profiles of plasma ions have often been measured to analyze ion temperature and density, plasma flow velocities, magnetic and electric field strengths, turbulence parameters [1–5]. An important disadvantage of spectroscopic measurements is that the line-integrals of local parameters are measured along a line of sight. This complicates the interpretation of the measured Doppler shift of the signals, which contain both plasma velocity and temperature information. Therefore, an inversion technique is needed, unless the line radiation is quite localized, to obtain the local parameter from the measurements. The well-known Abel inversion can be used to reconstruct the emissivity profile of plasmas with cylindrical symmetry, whereas scalar tomography methods are usually used in a non-symmetric case if effects of plasma motion are not taken into account [2,6,7]. However, in presence of plasma motion neither Abel inversion nor scalar tomography methods may be used because the emission of given wavelength is dependent on the orientation of line observation [3,4]. On the other hand, the plasma flow is one of the key issues to understand the confinement of tokamaks, such as the H-mode and the internal transport barrier. A large flow shear spreads out magnetic islands and suppresses the growth of plasma instabilities, improving plasma confinement. We developed a numerical method of vector tomography to be applied to plasma flow measurements by using spectral line measurements to extract the Doppler-shift of spectral lines. A cylindrical plasma boundary was used to demonstrate 2-D toroidal flow measurements for plasma toroids. A center-coil area is an opaque obstruction for emission radiation, and projections in this case will have data-missing parts. Our algorithm based on the maximum entropy principle was adopted for tomographic reconstruction from projections with data-missing parts. The main idea of modification comes from the Gerchberg [8] and Papoulis [9] algorithm and has been applied to tomography problems in [10]. This algorithm is based on the idea of "artificial" translucence of opaque medium, which means that the lost information concerning the data-missing part of one viewing position can be recovered by measured data from other directions. Iterative modifications using *a priori* information about the outline and the position of the opaque obstruction allow us to recover the surrounding part of the opaque obstruction. Other methods related to the problem with incomplete set of measurements are considered in [11–13].

In the first part of what follows we intend to show how the vector tomography equation can be derived for spectroscopic measurements. Part two describes the mathematical method for solving the vector tomography problem. Computer simulations are presented in part three. Our method enables us to reconstruct 2-D flow-lines or some specific component of flow velocity based on the assumption of plasma incompressibility $\operatorname{div} \mathbf{V} = 0$.

[a] e-mail: balandin@katsurai.t.u-tokyo.ac.jp
On leave from the Institute of System Dynamics and Control Theory, Irkutsk.
[b] e-mail: ono@katsurai.t.u-tokyo.ac.jp

2 Doppler spectroscopy

Suppose that plasma is optically thin, and it is assumed that the line width profile is predominantly caused by the Doppler broadening mechanism. The emissivity per unit volume at frequency ν, and position $\mathbf{x} = (x, y)$, and in the direction $\boldsymbol{\eta}$ is given by the following line integral over the ion velocity distribution function $f(\boldsymbol{\vartheta})$ in a velocity space [4,5]:

$$\varepsilon(\nu'; \mathbf{x}, \boldsymbol{\eta}) = \varepsilon_0(\mathbf{x}) \int_{-\infty}^{\infty} f(\boldsymbol{\vartheta}) \delta(\nu' - \boldsymbol{\vartheta} \cdot \boldsymbol{\eta}) \, \mathrm{d}\boldsymbol{\vartheta}, \qquad (1)$$

where $\varepsilon_0(\mathbf{x})$ is isotropic emission, $\boldsymbol{\vartheta}(\mathbf{x}) = \mathbf{V}(\mathbf{x})/c$ is a non-dimensional velocity field, $\nu' = (\nu - \nu_0)/\nu_0$ is a normalized frequency, ν_0 is the emission line center and c is the speed of light.

Under the conditions when self-absorption and refraction may be neglected, the intensity of radiation from the plasma $I_{\boldsymbol{\xi}}(\nu'; u)$ can be found simply by integrating the power emitted along the line of observation $L(u, \boldsymbol{\xi})$:

$$\begin{aligned} I_{\boldsymbol{\xi}}(\nu'; u) &= \int_{L(u,\boldsymbol{\xi})} \varepsilon(\nu'; \mathbf{x}, \boldsymbol{\eta}) \mathrm{d}l \\ &= \int_{\mathbf{R}^2} \varepsilon(\nu'; \mathbf{x}, \boldsymbol{\eta}) \delta(u - \mathbf{x} \cdot \boldsymbol{\xi}) \mathrm{d}\mathbf{x}, \end{aligned} \qquad (2)$$

where the unit vector $\boldsymbol{\eta}$ is orthogonal to the vector $\boldsymbol{\xi}$.

In special cases, when the particle velocity distribution is Maxwellian, the Doppler frequency shift results is a Gaussian line profile

$$\varepsilon(\nu'; \mathbf{x}, \boldsymbol{\eta}) = \frac{\varepsilon_0(\mathbf{x})}{\sqrt{2\pi} \Delta\nu'^2(\mathbf{x})} \exp\left(-(\nu' - \vartheta)^2 / 2\Delta\nu'^2\right), \qquad (3)$$

where $\vartheta = \boldsymbol{\vartheta} \cdot \boldsymbol{\eta}$ is the normalized Doppler frequency shift of the spectral line, and $\Delta\nu'$ is the line width. These are related to the plasma velocity and temperature of the radiating particles, respectively. Nonetheless, in the general case, the measured signal (2) along a sight line is not Gaussian and is dependent on the direction of observation at a given wavelength. Therefore, equation (2) cannot be directly inverted either by Abel's or by scalar tomography techniques [3]. However, some information can be obtained by integrating the spectral profile over the normalized frequency ν' [4]. By introducing the spectral moments of the line-integrated emission by the formula

$$\mu^{(n)} = \int_{-\infty}^{\infty} I_{\boldsymbol{\xi}}(\nu'; u) \, \nu'^n \mathrm{d}\nu', \qquad (4)$$

the following equalities can be obtained

$$\mu^{(0)} \equiv \mathcal{R}\{\varepsilon_0\}(u, \boldsymbol{\xi}) = \int_{L(u,\boldsymbol{\xi})} \varepsilon_0(\mathbf{x}) \, \mathrm{d}l, \qquad (5)$$

$$\mu^{(1)} \equiv \mathcal{V}\{\boldsymbol{\vartheta}\}(u, \boldsymbol{\eta}) = \int_{L(u,\boldsymbol{\xi})} \varepsilon_0(\mathbf{x}) \boldsymbol{\vartheta}(\mathbf{x}) \cdot \mathrm{d}\mathbf{l}, \qquad (6)$$

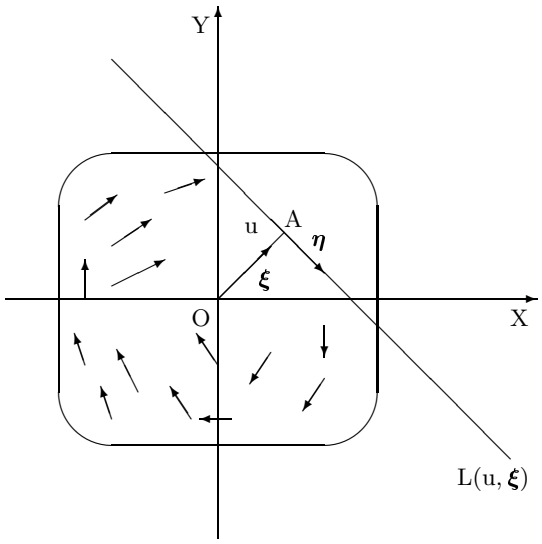

Fig. 1. The scheme of the data registration for the vector field. $\boldsymbol{\xi} \cdot \boldsymbol{\eta} = 0$, OA = u.

where $\mathcal{R}$ and $\mathcal{V}$ denote scalar and vectorial (see definition below) Radon transformations, respectively. The vectors $\boldsymbol{\xi}$, $\boldsymbol{\eta}$ and the variable u are shown in Figure 1. Equation (5) shows that the isotropic emissivity $\varepsilon_0(\mathbf{x})$ can be determined by scalar tomography methods, whereas equation (6) is related to the tomography of vector fields and requires special inversion methods.

3 Inversion method

Assume that $\varepsilon_0(\mathbf{x})$ is known as the solution of equation (5). Without any loss of generality, equation (6) can be considered in the following form and will further be called the vectorial Radon transform

$$\mathcal{V}\{\boldsymbol{\vartheta}\}(u, \boldsymbol{\eta}) = \int_{L(u,\boldsymbol{\xi})} \boldsymbol{\vartheta}(\mathbf{x}) \cdot \mathrm{d}\mathbf{l}, \qquad (7)$$

where vector $\boldsymbol{\eta}$ is the unit vector along the line of observation and orthogonal to the vector $\boldsymbol{\xi}$.

For the measurements in the two-dimensional space, the geometry of data registration is outlined in Figure 1. The unit vector $\boldsymbol{\xi}$ is defined as $\boldsymbol{\xi} = (\cos\theta, \sin\theta)$, and θ is an angle between the positive direction X-axis and the line OA. The problem in this case may be conveniently considered in terms of the vorticity vector function $\boldsymbol{\zeta} = \operatorname{curl} \boldsymbol{\vartheta}$, which has only one component $\boldsymbol{\zeta} = (0, 0, \zeta)$ and ζ is defined conventionally as

$$\zeta(x, y) = \frac{\partial \vartheta_y}{\partial x} - \frac{\partial \vartheta_x}{\partial y}, \qquad (8)$$

where ϑ_x and ϑ_y are the components of a vector field $\boldsymbol{\vartheta}$.

The following proposition (9) can be easily proved. For the first time this result in the Fourier space for a two-dimensional vector field was given in [14]

$$\frac{\partial}{\partial u} \mathcal{V}\{\boldsymbol{\vartheta}\}(u, \boldsymbol{\eta}) = \mathcal{R}\{\zeta\}(u, \boldsymbol{\eta}). \qquad (9)$$

To obtain the velocity field out of the vorticity distribution it is necessary to use Helmholtz's decomposition theorem

$$\boldsymbol{\vartheta} = \operatorname{curl} \boldsymbol{\Psi} + \operatorname{grad} \Phi, \tag{10}$$

where $\boldsymbol{\Psi}$ and Φ are, respectively, the vector and scalar potential functions, and $\operatorname{curl} \boldsymbol{\Psi}$ and $\operatorname{grad} \Phi$ are, respectively, the solenoidal and irrotational parts of $\boldsymbol{\vartheta}$. Since $\boldsymbol{\vartheta}$ is confined to the $x-y$-plane, a single component of the vector potential $\boldsymbol{\Psi}$ in the z-direction is sufficient to define $\operatorname{curl} \boldsymbol{\Psi}$ uniquely; *i.e.* one can write $\boldsymbol{\Psi} = \psi\, \mathbf{e}_z$. Thus, in two dimensions, $\boldsymbol{\vartheta}(x, y)$ is completely determined by the two scalar functions $\Phi(x, y)$ and $\psi(x, y)$. The velocity components write

$$\vartheta_x = \frac{\partial \psi}{\partial y} + \frac{\partial \Phi}{\partial x}, \quad \vartheta_y = -\frac{\partial \psi}{\partial x} + \frac{\partial \Phi}{\partial y}, \tag{11}$$

and after substitution in (8) one obtains

$$\nabla^2 \psi = -\zeta. \tag{12}$$

Using the following Radon transform property [15]

$$\mathcal{R}\{\nabla^2 f(\mathbf{x})\} = \frac{\partial^2 \mathcal{R}\{f\}}{\partial u^2},$$

equation (9) may be rewritten as follows

$$\mathcal{V}\{\boldsymbol{\vartheta}\}(u, \boldsymbol{\eta}) = -\frac{\partial}{\partial u} \mathcal{R}\{\psi\}(u, \boldsymbol{\eta}), \tag{13}$$

or in the form

$$\mathcal{R}\{\psi\}(u, \boldsymbol{\eta}) = -\int_{-\infty}^{u} \mathcal{V}\{\boldsymbol{\vartheta}\}(u', \boldsymbol{\eta}) \mathrm{d}u'. \tag{14}$$

The approach to inversion of the vectorial Radon transform is now reduced to a scalar Radon inversion of integrated measured data, and any algorithm of scalar tomography can now be applied for determination of the ψ-function. Equation (14) shows that only the solenoidal component ψ (and hence, $\operatorname{curl} \boldsymbol{\Psi}$) is determined uniquely from the line-integrated data. There is no contribution from the irrotational component $\operatorname{grad} \Phi$ in equation (14). This allows to reconstruct the solenoidal component independently of the irrotational component. As shown for the first time in [14], the component $\operatorname{grad} \Phi$ can be recovered from the boundary values of $\boldsymbol{\vartheta}$. Now assume that only solenoidal motion is present, *i.e.* the velocity components are defined as follows

$$\vartheta_x = \frac{\partial \psi}{\partial y}, \quad \vartheta_y = -\frac{\partial \psi}{\partial x}\,.$$

Several models for the z-component of the vector potential ψ, and its reconstructions by the line-integrated data will be considered in the next section. Any suitable algorithm for scalar tomography can now be applied for the determination of the ψ-function from equation (14). The generalized maximum entropy method was developed for this problem. It was discussed in detail in [16], and a brief explanation is given in Appendix B.

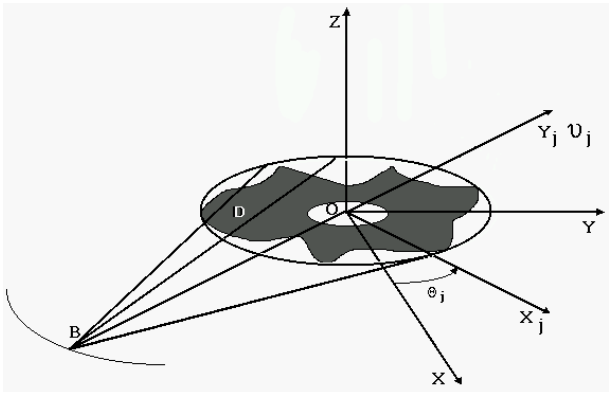

Fig. 2. The fan beam scheme at one of the positions of registration of the projections. The detector position is defined by the distance OB $= d$ and by the angle θ_j between the positive directions of X- and X_j-axes.

4 Computer simulation

For these simulations we will consider a vector field with the vector potential $\boldsymbol{\Psi}$. In the two-dimensional space the potential $\boldsymbol{\Psi}$ has only one component and writes $\boldsymbol{\Psi} = (0, 0, \psi)$, where ψ is chosen of the form

$$\psi(\rho) = \exp\left(-\frac{(\rho - \rho_0)^2}{2\sigma^2}\right), \tag{15}$$

where ρ is the radius in a polar system of coordinates, ρ_0 defines the shift of the Gaussian function. We can get the models, which are either peaked if $\rho_0 = 0$ or hollow if $\rho_0 \neq 0$. The corresponding vector field is given by the components

$$v_x = \exp\left(-\frac{(\rho - \rho_0)^2}{2\sigma^2}\right)\left(-\frac{y(\rho - \rho_0)}{\rho\sigma^2}\right)$$
$$v_y = \exp\left(-\frac{(\rho - \rho_0)^2}{2\sigma^2}\right)\left(\frac{x(\rho - \rho_0)}{\rho\sigma^2}\right).$$

In the process of computations it is more suitable to use the half-width $\Delta\rho = 2\sqrt{(2 \ln 2)}\ \sigma$ rather than σ in (15). We plan to use this tomography diagnostics for the spherical tokamak TS-4 [17]. The device TS-4 was used as a sort of prototype. The developed method can easily be extended to any spherical tokamak experiment with various geometry of measurements. The spherical tokamak TS-4 can produce one or two spherical tokamaks of major radius of 0.5 m and aspect ratio of 1.2–1.9 inside its cylindrical vacuum vessel having the length of 2 m and the diameter of 1.8 m. Its spectrum line emission of various impurity species can be measured by detectors located inside and outside of the vacuum vessel. If the measurements are performed at the plane $z = const$ as in Figure 2, where z is the axis of device symmetry, the information about toroidal flow velocity can be extracted from the data. On the other hand, if detectors are located along the axis z of the vacuum vessel, one can obtain information about a poloidal vector field. Owing to the two different models (peaked and hollow) we have examined the algorithm

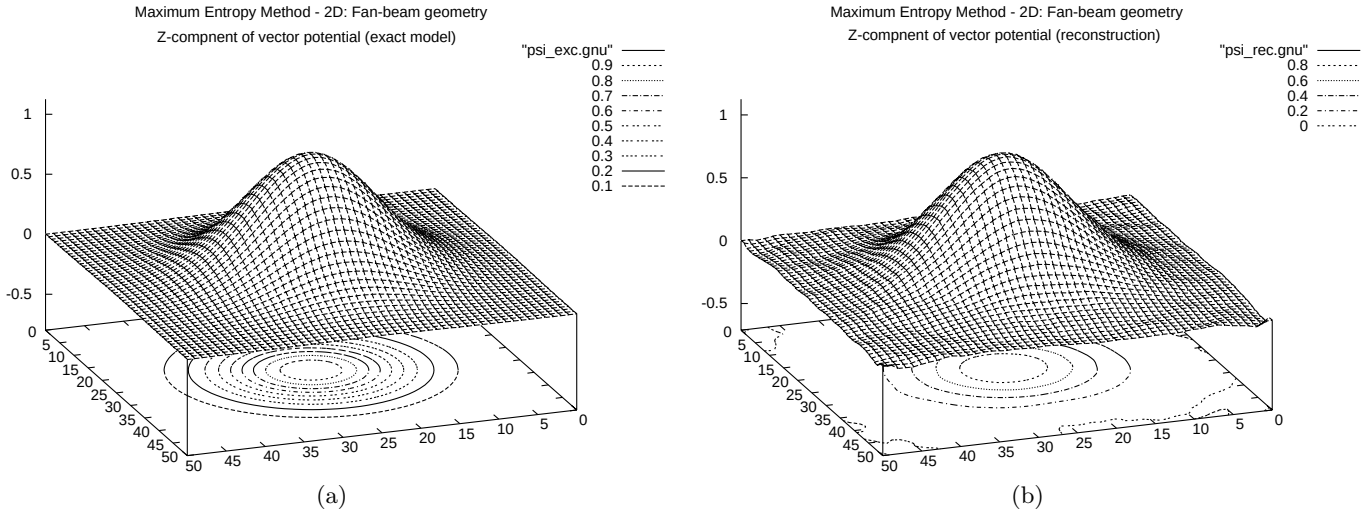

(a) (b)

Fig. 3. The first model of ψ-function; exact, (a), and reconstructed, (b). $\rho_0 = 0.0, \Delta\rho = 0.55$. Relative error of reconstruction is 1.2%.

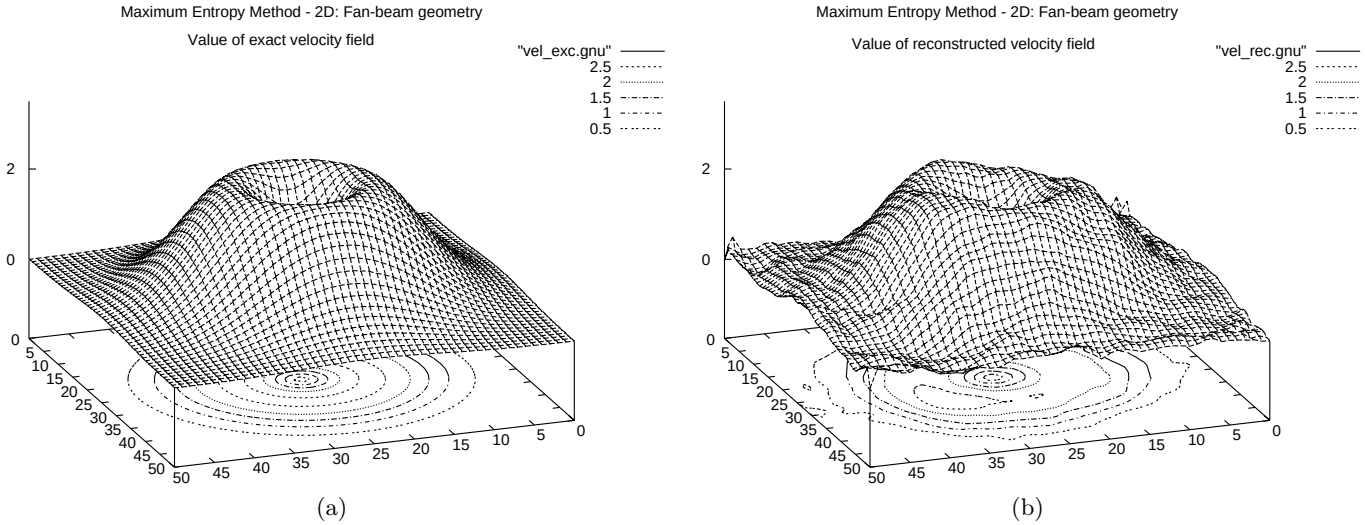

(a) (b)

Fig. 4. The values of the vector field for the first model: exact, (a), reconstructed, (b). $\rho_0 = 0.0, \Delta\rho = 0.55$.

using the scheme of measurements as shown in Figure 2. In the both numerical experiments the total number of 10 1-D projections were used, each of them containing 51 ray-sums. The noise level was taken to be 5% and 10% of the maximum level of measured data (projections). The reconstruction errors, which depend on a number of projections and level of noise for the first (—○—, —∗—) and the second (—+—, —◇—) models, are given in Figure 9. The detectors were located uniformly in $\theta_j \in [0, \pi]$. The reconstruction was performed inside the circle of normalized radius $R = 1$. An exact and reconstructed ψ-function are drawn in Figures 3a, 3b, 6a and 6b. With noise added to the projection data, the relative error of reconstruction is 1.2% for the first and about 17% for the second model, respectively. The vector fields, exact and reconstructed, corresponding to those of two ψ-functions, are shown in Figures 5a, 5b, 8a and 8b. In Figures 4a, 4b, 7a and 7b the values $|\boldsymbol{\vartheta}(x, y)| = \vartheta_x^2 + \vartheta_y^2$ of these vector fields are shown.

5 Conclusion

In this paper, a unique numerical method for reconstructing the vector potential of a plasma velocity field has been proposed. It has been developed by applying a vectorial Radon transform to spectroscopic measurements. The components of the vector field are recovered by differentiation of a single component of the vector potential. A special modification of the maximum entropy method for sign-altering functions was implemented for the inversion of the vectorial Radon transform. An alternative approach could be used for reconstructing the vorticity field by direct differentiation of (9). But in this case, the

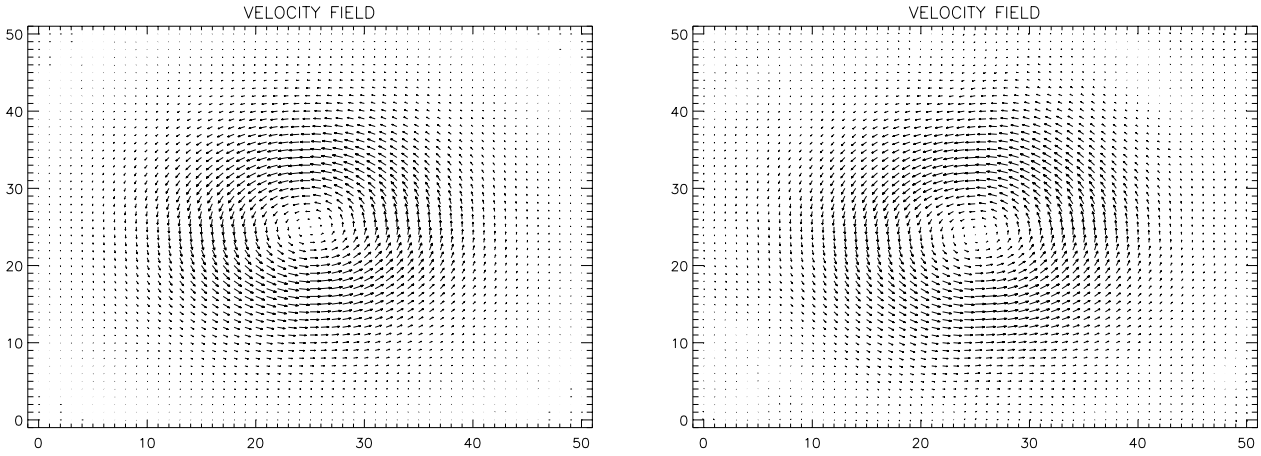

(a) (b)

Fig. 5. The velocity vector field for the first model: exact, (a), and reconstructed, (b). $\rho_0 = 0.0, \Delta\rho = 0.55$.

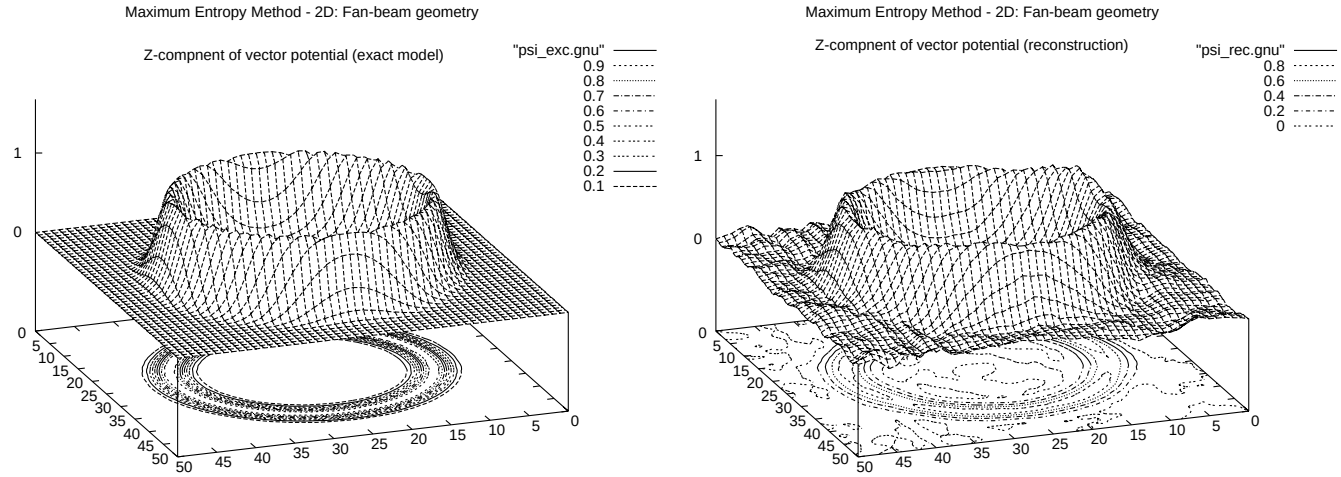

(a) (b)

Fig. 6. The second model of ψ-function: exact, (a), and reconstructed, (b). $\rho_0 = 0.45, \Delta\rho = 0.1$. The relative error of the reconstructed entity is 11%.

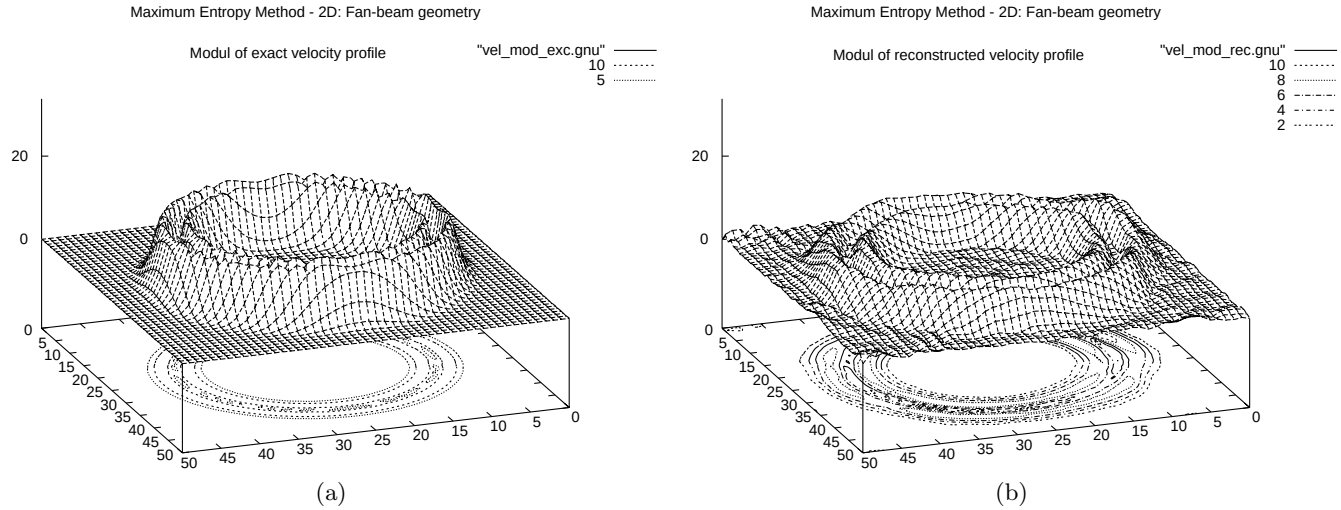

(a) (b)

Fig. 7. The value of the vector field for the second model: exact, (a), reconstructed, (b). $\rho_0 = 0.45, \Delta\rho = 0.1$.

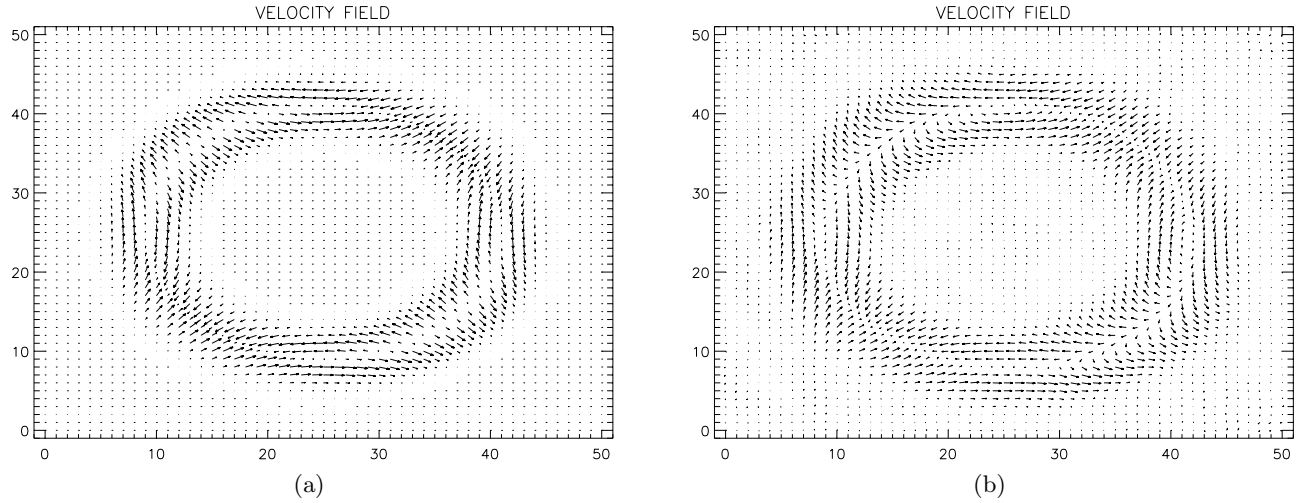

Fig. 8. The velocity vector field for the second model: exact, (a), and reconstructed, (b). $\rho_0 = 0.45, \Delta\rho = 0.1$.

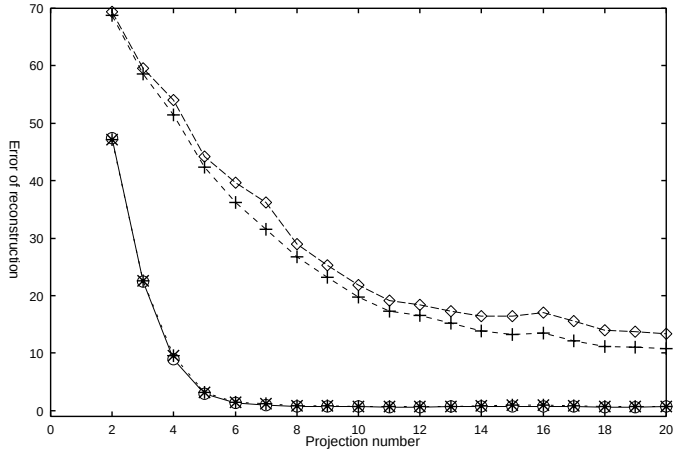

Fig. 9. The error of reconstruction (per cent) of ψ-function depending on the number of projections and the level of noise; the noise of 5% (—○—), (—+—) and the noise of 10% (—∗—), (—◇—) for the first and the second models, respectively.

experimental data should be differentiated, and instability of this procedure requires a regularization technique to obtain a robust solution. As a result of computer simulation, the reconstruction error observed was found to be substantially dependent on the type of the model, on the number of projections, and it is quite robust to the level of noise (see Fig. 9). The technique developed is means to be used for plasma flow velocity reconstruction in the spherical tokamak TS-4, and can easily be extended not only to other spherical toroidal plasmas but also to all kinds of toroidal plasmas.

The first author would like to express his gratitude to the staff of High-Temperature Plasma Center, University of Tokyo, for their great hospitality. The work was partially supported by the RFBR, project No. 00-01-00219.

Appendix A

A.1 Maximum entropy inversion method (MEM)

In this section we briefly consider a version of MEM adapted to sign-altering functions. Because the right part of (14) may contain a negative values, the MEM should be modified for this case. The scalar function $g(\mathbf{x})$ used in this section corresponds to the ψ-function in equation (14). The geometry of measurement and an appropriate coordinate systems are shown in Figure 2. We assume that the unknown source function $g(\mathbf{x})$ is continuous and has a compact support D. It is convenient to employ a different frame of reference for each fan beam.

Let $\mathbf{x} = (x, y)$ be Cartesian coordinates. For the jth fan beam we introduce the rotated frame of reference $\mathbf{x}_j = (x_j, y_j)$ as follows

$$\mathbf{x}_j = R_j \mathbf{x}.$$

For the two-dimensional case the matrix of rotation R_j writes

$$R_j = \begin{pmatrix} \cos\theta_j & \sin\theta_j \\ -\sin\theta_j & \cos\theta_j \end{pmatrix}.$$

We also introduce, following [19], the fan coordinates (u, v) with the vertex at $y = -d$ by the transformation formulas

$$u = \frac{x}{1 + y/d}, \qquad x = u(1 + v/d),$$
$$v = y, \qquad y = v.$$

Applying this transformation to the rotated system of coordinates (x_j, y_j) we obtain

$$u_j = \frac{x_j}{1 + y_j/d}, \qquad x_j = u_j(1 + v_j/d),$$
$$v_j = y_j, \qquad y_j = v_j.$$

The functional dependence, direct and inverse, respectively, between (u_j, v_j) and (x, y) defined as above will

be expressed for $j = 1, 2, ..., J$ in the form

$$u_j = U_j(x, y), \quad x = X_j(u, v),$$
$$v_j = V_j(x, y), \quad y = Y_j(u, v).$$

Without any loss of generality we can assume that the measured data of the jth fan beam are known along the x_j-axis. The relation between the unknown source function $g(x, y)$ and the projection functions $G_j(u)$ measured along the axis x_j is

$$G_j(u) = \int_{R^2} \mathrm{d}\mathbf{x}\, g(\mathbf{x})\, \delta\big(u - U_j(\mathbf{x})\big) = \int_{-\infty}^{\infty} \mathrm{d}v \left|\frac{\partial(x, y)}{\partial(u, v)}\right| g\big(X_j(u, v), Y_j(u, v)\big), \quad (16)$$

where

$$\mathcal{J} = \frac{\partial(x, y)}{\partial(u, v)} = \begin{vmatrix} \frac{\partial x}{\partial u} & \frac{\partial y}{\partial u} \\ \frac{\partial x}{\partial v} & \frac{\partial y}{\partial v} \end{vmatrix} = 1 + v/d.$$

Let g_+ and g_- be the two positive functions bound up with g as follows:

$$g_+(\mathbf{x}) = \begin{cases} g(\mathbf{x}), & \text{if} \quad g(\mathbf{x}) > 0; \\ 0, & \text{if} \quad g(\mathbf{x}) \le 0; \end{cases} \quad (17)$$

$$g_-(\mathbf{x}) = \begin{cases} -g(\mathbf{x}), & \text{if} \quad g(\mathbf{x}) < 0; \\ 0, & \text{if} \quad g(\mathbf{x}) \ge 0. \end{cases} \quad (18)$$

Using the Lagrangian method of multipliers, the problem of determination of the function g is reduced to the unconstrained maximization of the Lagrange functional

$$L(g, \boldsymbol{\Lambda}) = \eta(g) - \sum_{j=1}^{J} \int_{-\infty}^{\infty} \mathrm{d}u\, \Lambda_j(u) \tilde{G}_j(u) \quad (19)$$

$$\tilde{G}_j(u) = G_j(u) - \int_{-\infty}^{\infty} \mathrm{d}v\, |\mathcal{J}| (g_+(X_j, Y_j) - g_-(X_j, Y_j))$$

where $\boldsymbol{\Lambda} = (\Lambda_j),\ j = 1, \ldots, J$ are Lagrange multipliers, $X_j = X_j(u, v)$, $Y_j = Y_j(u, v)$. The entropy functional $\eta(g)$ is defined as follows

$$\eta(g) = -\iint_{\mathrm{D}} \mathrm{d}x\, \mathrm{d}y \left(g_+(x, y) \ln(g_+(x, y)/V_+) + g_-(x, y) \ln(g_-(x, y)/V_-)\right), \quad (20)$$

where V_+ and V_- are the constants representing an *a priori* magnitude for the positive, resp., negative part of g. Initially we put $V_- = V_+$. The replacement of the variables transforms the second integral to the form

$$\int_{-\infty}^{\infty} \mathrm{d}u \Lambda_j(u) \int_{-\infty}^{\infty} \mathrm{d}v\, |\mathcal{J}|\, (g_+(X_j, Y_j) - g_-(X_j, Y_j)) = \iint_D \mathrm{d}x\, \mathrm{d}y\, g(x, y) \Lambda_j(U_j(x, y)).$$

Taking the variations of $L(g, \boldsymbol{\Lambda})$ with respect to the functions g_+ and g_-, and equating each of the former to zero, we obtain

$$g_+(x, y) = V'_+ \prod_{l=1}^{J} H_l\big(U_l(x, y)\big), \quad (21a)$$

$$g_-(x, y) = V'_- \prod_{l=1}^{J} \frac{1}{H_l\big(U_l(x, y)\big)}, \quad (21b)$$

where $H_l(\cdot) \equiv \exp(\Lambda_l(\cdot))$ and $V'_+ = V_+/\mathrm{e}$, $V'_- = V_-/\mathrm{e}$, $\mathrm{e} = 2.71828...$ are constants. The unknown functions $H_j(\cdot)$ are determined now *via* the substitution of (21a) and (21b) into the constraints (16):

$$G_j(u) = \int_{-\infty}^{\infty} \mathrm{d}v\, |\mathcal{J}| \prod_{l=1}^{J} \Big\{ V'_+ H_l\big(U_l(X_j(u, v), Y_j(u, v))\big) - \frac{V'_-}{H_l\big(U_l(X_j(u, v), Y_j(u, v))\big)} \Big\} = \int_{-\infty}^{\infty} \mathrm{d}v\, |\mathcal{J}| \prod_{l=1}^{J} \Big\{ V'_+ H_l\big(U_{lj}(u, v)\big) - \frac{V'_-}{H_l\big(U_{lj}(u, v)\big)} \Big\}, \quad (22)$$

where $U_{lj}(u, v) \equiv U_l(X_j(u, v), Y_j(u, v))$.

The following equations for the functions H_j are obtained

$$G_j(u) = V'_+ H_j(u)\, h_1(u) - \frac{V'_- h_2(u)}{H_j(u)}, \quad (23a)$$

$$h_1(u) = \int_{-\infty}^{\infty} \mathrm{d}v \left|1 + v/d\right| \prod_{l \ne j}^{J} H_l\big(U_{lj}(u, v)\big), \quad (23b)$$

$$h_2(u) = \int_{-\infty}^{\infty} \mathrm{d}v \left|1 + v/d\right| \prod_{l \ne j}^{J} \frac{1}{H_l\big(U_{lj}(u, v)\big)}. \quad (23c)$$

This algebra leads to the following iteration scheme

$$H_j^{i+1}(u) = \frac{G_j(u)}{2h_1^i(u)V'_+} + \left[\left(\frac{G_j(u)}{2h_1^i(u)V'_+}\right)^2 + \frac{h_2^i(u)V'_-}{h_1^i(u)V'_+}\right]^{1/2}, \quad \text{for} \quad j = i \pmod J + 1; \quad (24a)$$

$$H_j^{i+1}(u) = H_j^i(u), \quad \text{for} \quad j \ne i \pmod J + 1; \quad (24b)$$

$$H_j^0(u) = \begin{cases} 1, & \text{if} \quad G_j(u) \ne 0, \\ 0, & \text{if} \quad G_j(u) = 0. \end{cases} \quad (24c)$$

This describes the main part of the inversion algorithm. The idea of "artificial" translucence is realized in the following way. At first, the missing data at the projections are recovered by any method of interpolation. The above inversion algorithm is applied to get some estimation of

emissivity distribution. After that, the projection data are computed numerically, and only the shadowed part of the projections is retained, any other values are taken from the experimental data to be used. On this step, any *a priori* information may be added, for instance – positiveness.

References

1. E. Oks, *Plasma Spectroscopy: The Influence of Microwave and Laser Fields* (Springer Series on Atoms and Plasma Berlin, 1995), N. 9.
2. E.I. Kuznetsov, D.A. Shcheglov, *High Temperature Plasma Diagnostic* (Atomizdat, Moscow, 1980) (in *Russian*).
3. R.E. Bell, Rev. Sci. Instrum. **68**, 1273 (1997).
4. J. Howard, Plasma Phys. Control. Fusion **38**, 489 (1996).
5. R.S. Shaw, J. Opt. Soc. Am. A **4**, 2254 (1987).
6. C.D. Maldonado, A.P. Caron, H.N. Olsen, J. Opt. Soc. Am. **55**, 1247 (1965).
7. C.D. Maldonado, H.N. Olsen, J. Opt. Soc. Am. **56**, 1305 (1966).
8. R.W. Gerchberg, Opt. Acta **21**, 709 (1974).
9. A.A. Papoulis, IEEE Trans. Circ. Syst. **22**, 735 (1975).
10. A.L. Balandin, V.V. Pickalov, N.G. Preobrazhensky, in *Proceedings of the IV All-Union Symposium on Computerized Tomography*, 1989, edited by M.M. Lavrentiev, Novosibirsk, p. 68 (in *Russian*).
11. B.E. Oppenheim, IEEE Trans. Nucl. Sci. **21**, 72 (1974).
12. R.M. Lewitt, R.H. Bates, Optik **50**, 189 (1978).
13. R.M. Lewitt, R.H. Bates, Optik **50**, 269 (1978).
14. S.J. Norton, Gophys. J. **97**, 161 (1988).
15. S.R. Deans, *The Radon transform and some of its applications* (John Wiley & Sons, New-York, 1983).
16. A.L. Balandin, A. Kaneko, Inv. Probl. **15**, 445 (1999).
17. Y. Ono, M. Inomoto, Phys. Plasmas **7**, 1863 (2000).
18. F. Natterer, *The Mathematics of Computerized Tomography* (John Wiley & Sons Ltd and B.G. Teubner, Stuttgart, 1986).
19. G. Minerbo, Comput. Biol. Med. **9**, 29 (1979).
20. M.S. Bazaraa, C.M. Shetty, *Foundations of optimization* (Springer-Verlag, Berlin, New York, 1976).